Supplementary Information: Fröhlich polaron effective mass and localization length in cubic materials: degenerate and anisotropic electronic bands

Bogdan Guster,[1] Pedro Melo,[2] Bradley A. A. Martin,[3] Véronique Brousseau-Couture,[4] Joao C. de Abreu,[2] Anna Miglio,[1] Matteo Giantomassi,[1] Michel Côté,[5] Jarvist M. Frost,[3] Matthieu J. Verstraete,[2] and Xavier Gonze[1,6]

[1]*European Theoretical Spectroscopy Facility, Institute of Condensed Matter and Nanosciences, Université catholique de Louvain, Chemin des étoiles 8, bte L07.03.01, B-1348 Louvain-la-Neuve, Belgium*

[2]*NanoMat/Q-Mat/CESAM and European Theoretical Spectroscopy Facility, Université de Liège (B5), B-4000 Liège, Belgium*

[3]*Department of Physics, Imperial College London, Exhibition Road, London SW7 2AZ, UK*

[4] *Département de Physique et Regroupement Québécois sur les Matériaux de Pointe, Université de Montreal, C.P. 6128, Succursale Centre-Ville, Montreal, Canada H3C 3J7*

[5] *Département de Physique, Université de Montreal, C.P. 6128, Succursale Centre-Ville, Montreal, Canada H3C 3J7*

[6]*Skolkovo Institute of Science and Technology, Skolkovo Innovation Center, Nobel St. 3, Moscow, 143026, Russia.*

(Dated: November 22, 2021)

PACS numbers: 71.20.Ps, 78.20.-e, 42.70.-a

(I) Supplementary theory

(II) Supplementary figures

(III) Supplementary tables

I. SUPPLEMENTARY THEORY

A. Polaron localization length asymptotic behavior in the uniaxial limit

Based on the electronic effective masses, we provide analytical formulas for the asymptotic behaviour of the localization lengths in the non-degenerate anisotropic case. We determine the spherical average asymptotic behaviour in the low limit of μ^* (as defined in the main text), Eq. S1, respectively high limit - Eq. S5. Similarly, we follow with the two meaningful localization lengths a_{p_z} (Eq. S2 and Eq. S6), respectively $a_{p_\perp}$ (Eq. S3 and Eq. S7), and polaron formation energy (Eq. S4 and Eq. S8).

$$\lim_{\mu^*\to 0} a_P = 2\Big(\frac{\pi}{2}\Big)^{-5/2} m_\perp^{-1}\epsilon^*\Big(\frac{\pi\mu^*}{4}\Big)^{1/9} \tag{S1}$$

$$\lim_{\mu^*\to 0} a_{P_z} = 2\Big(\frac{\pi}{2}\Big)^{-5/2} m_\perp^{-1}\epsilon^*\Big(\frac{\pi\mu^*}{4}\Big)^{1/3} \tag{S2}$$

$$\lim_{\mu^*\to 0} a_{P_\perp} = 2\Big(\frac{\pi}{2}\Big)^{-5/2} m_\perp^{-1}\epsilon^* \tag{S3}$$

$$\lim_{\mu^*\to 0} E_P(\mu^*) = -\frac{\pi}{16} m_\perp^*(\epsilon^*)^{-2} \tag{S4}$$

$$\lim_{\mu^*\to \infty} a_P = 4\sqrt{2\pi} m_z^{-1}(\mu^*)2/3\epsilon^*(\log(4\mu^*))^2(\log(4\mu^*))^{-2}(\log(4\mu^2) - 2 - \log(\log(4\mu^*) - 2))^{-2/3} \tag{S5}$$

$$\lim_{\mu^*\to \infty} a_{P_z} = 4\sqrt{2\pi} m_z^{-1}\mu\epsilon^*(\log(4\mu^*))^2(\log(4\mu^*))^{-2}(\log(4\mu^2) - 2 - \log(\log(4\mu^*) - 2))^{-1} \tag{S6}$$

$$\lim_{\mu^*\to\infty} a_{P_\perp} = 4\sqrt{2\pi}m_z^{-1}(\mu^*)^{1/2}\epsilon^*(\log(4\mu^*))^2(\log(4\mu^*))^{-2}(\log(4\mu^2)-2-\log(\log(4\mu^*)-2))^{-1/2} \tag{S7}$$

$$\lim_{\mu^*\to\infty} E_P(\mu^*) = -\frac{1}{8\pi}m_z(\epsilon^*)^{-2}(\log(4)+\log(\mu^*))^2 \tag{S8}$$

In our representation inside the main text we are working at a constant density of states, thus we can define the effective mass in the following way, considering that $m_x = m_y = m_\perp$:

$$m^*_{DoS} = (m_x m_y m_z)^{1/3} \tag{S9}$$

$$m_z = m^*_{DoS}(\mu^*)^{-2/3} \tag{S10}$$

$$m_\perp = m^*_{DoS}(\mu^*)^{1/3} \tag{S11}$$

Consequently, the asymptotic behaviour for the different localization lengths and formation energy are defined as:

$$\lim_{\mu^*\to 1} a_P = \frac{3}{2}\sqrt{2\pi}m^{-1}_{DoS}\epsilon^*\Big(1+\frac{3}{14}(\mu^*-1)\Big) \tag{S12}$$

$$\lim_{\mu^*\to 1} a_{P_z} = \frac{3}{2}\sqrt{2\pi}m^{-1}_{DoS}\epsilon^*\Big(1+\frac{2}{21}(\mu^*-1)\Big) \tag{S13}$$

$$\lim_{\mu^*\to 1} a_{P_\perp} = \frac{3}{2}\sqrt{2\pi}m^{-1}_{DoS}\epsilon^*\Big(1+\frac{19}{42}(\mu^*-1)\Big) \tag{S14}$$

$$\lim_{\mu^*\to 1} E_p(\mu^*) = -\frac{1}{6\pi}m^*_{DoS}(\epsilon^*)^{-2} \tag{S15}$$

B. Polaron properties in the ellipsoidal limit

In the case of the tri-axial ellipsoidal limit we provide an approximate solution to the polaron localization length and formation energy. We base our estimation on the formalism provided in the asymptotic non-degenerate case where we have the exact solution for the cases of $m^*_x = m^*_y \neq m^*_z$ (and their commutative counterparts). Thus we estimate the average localization length in the cases where $m^*_x \neq m^*_y \neq m^*_z$ considering a cosine interpolation function, as defined in Eq. S18, while working under the constant volume condition, as defined in Eq. S16.

$$a_P = (a_{Px}a_{Py}a_{Pz})^{1/3} \tag{S16}$$

$$\delta_\sigma = \exp\left(\sigma\sqrt{6}|c|\right) - 1; \sigma = \pm \tag{S17}$$

$$\ln < a >= \ln a_P - \frac{1}{2}\sum_{\sigma=\pm}(1+\sigma\cos(3\theta))(1+\delta_\sigma)^{1/6}S(\delta_\sigma) \tag{S18}$$

$$|c| = \left(\frac{2}{3}\Big(\ln^2 a_{Px} + \ln^2 a_{Py} + \ln^2 a_{Pz} - \ln a_{Px}\ln a_{Py} - \ln a_{Py}\ln a_{Pz} - \ln a_{Pz}\ln a_{Px}\Big)\right)^{1/2} \tag{S19}$$

$$\frac{\partial \ln < a >}{\partial a_{Pz}} = 3a_{Pz} + + \frac{1}{2}\sum_{\sigma=\pm}\left\{\frac{\partial}{\partial a_{Pz}}(\cos(3\theta))\sigma(1+\delta_\sigma)^{1/6}S(\delta_\sigma) + (1+\sigma\cos(3\theta))\frac{\partial}{\partial a_{Pz}}\Big[(1+\sigma_\delta)^{1/6}S(\delta_\sigma)\Big]\right\} \tag{S20}$$

$$cos(3\theta) = \frac{4}{(\sqrt{6}|c|)^3}\ln\Big(\frac{a_{Px}a_{Py}}{a_{Pz}^2}\Big)\ln\Big(\frac{a_{Pz}a_{Px}}{a_{Py}^2}\Big)\ln\Big(\frac{a_{Py}a_{Pz}}{a_{Px}^2}\Big) \tag{S21}$$

$$\frac{\partial}{\partial a_{Pz}}(\cos(3\theta)) = \cos(3\theta)\left[-\frac{3}{|c|}\frac{\partial|c|}{\partial a_{Pz}} + a_{Pz}\left(\ln\Big(\frac{a_{Px}a_{Pz}}{a_{Py}^2}\Big)^{-1} + \ln\Big(\frac{a_{Py}a_{Pz}}{a_{Px}^2}\Big)^{-1} - 2\ln\Big(\frac{a_{Px}a_{Py}}{a_{Pz}^2}\Big)^{-1}\right)\right] \tag{S22}$$

$$\frac{\partial|c|}{\partial a_{Pz}} = \frac{a_{Pz}}{|c|}\ln\Big(\frac{a_{Pz}^2}{a_{Px}a_{Py}}\Big) \tag{S23}$$

$$\frac{\partial}{\partial a_{Pz}}\Big[(1+\delta_\sigma)^{1/6}S(\delta_\sigma)\Big] = \frac{\partial\delta_\sigma}{\partial a_{Pz}}\Big[\frac{1}{6}(1+\delta_\sigma)^{-5/6}S(\delta_\sigma) + (1+\delta_\sigma)^{1/6}\frac{dS}{d\delta}\Big|_{\delta_\sigma}\Big] \tag{S24}$$

$$\frac{\partial\delta_\sigma}{\partial a_{Pz}} = \sigma\sqrt{6}(\delta_\sigma+1)\frac{\partial|c|}{\partial a_{Pz}} \tag{S25}$$

II. SUPPLEMENTARY FIGURES

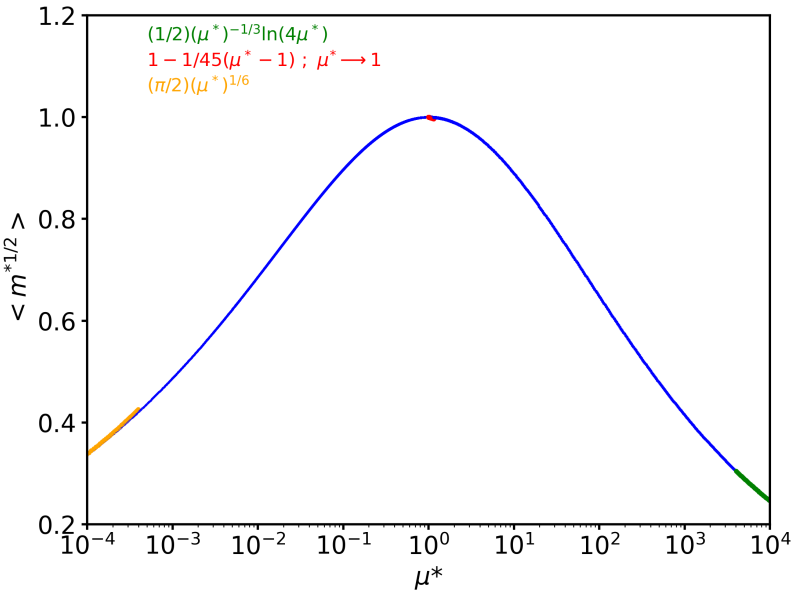

FIG. S1: Average squared effective mass in the uniaxial limit calculated at constant density of states expressed in terms of μ^*. In the low limit of μ^* , the asymptotic analytical behaviour is represented in orange. In the $\mu^* \to 1$ limit, the analytical expression is represented in red. Finally, in the large μ^* limit, the asymptotic behaviour analytical limit is represented in green. We consider here $\epsilon^* = 1$.

III. SUPPLEMENTARY TABLES

TABLE S1: *ab initio* DFT convergence parameters for the studied materials such as: kinetic energy cut-off in the plane-wave basis set, electronic states wavevector (k-point) sampling.

Material	Ecut(Ha)	k-point sampling
AlAs	40	6x6x6 (x4 shifts)
AlN	35	6x6x6
AlP	25	8x8x8 (x4 shifts)
AlSb	40	6x6x6 (x4 shifts)
BAs	40	6x6x6 (x4 shifts)
BN	35	8x8x8
CdS	45	6x6x6 (x4 shifts)
CdSe	50	6x6x6 (x4 shifts)
CdTe	50	6x6x6 (x4 shifts)
GaAs	40	6x6x6 (x4 shifts)
GaN	40	6x6x6 (x4 shifts)
GaP	40	6x6x6 (x4 shifts)
SiC	35	6x6x6 (x4 shifts)
ZnS	40	6x6x6 (x4 shifts)
ZnSe	40	6x6x6 (x4 shifts)
ZnTe	40	6x6x6 (x4 shifts)
BaO	40	8x8x8
CaO	40	8x8x8
Li2O	50	8x8x8
MgO	50	8x8x8 (x4shifts)
SrO	40	8x8x8

TABLE S2: Density functional theory calculated band parameters for triply degenerate valence bands given as Luttinger parameters, and non-degenerate anisotropic conduction bands given as electronic effective masses. In all calculation the theoretical lattice parameters were used, except for GaP where the experimental lattice parameter extrapolated at 0 K was used. The position of the band gap is also indicated.

Material	cell(Bohr)	VB - Luttinger Param			CB - Eff. masses		Gap
		A	B	C	$m_\perp$	m_z	
AlAs	10.825	-4.681	-1.019	-5.498	0.243	0.897	Γ-X
AlN	8.130	-1.435	-0.351	-1.793	0.321	0.520	Γ-X
AlP	10.406	-2.598	-0.894	-3.335	0.252	0.809	Γ-X
AlSb	11.762	-6.473	-1.372	-7.520	0.222	1.142	Γ-L
BaAs	9.088	-2.337	-2.104	-3.912	0.216	1.094	Γ-Δ
BN	6.746	-0.917	-0.969	-1.635	0.299	0.895	Γ-X
CdS	11.202	-3.999	-0.605	-4.321	0.118	0.118	Γ-Γ
CdSe	11.711	-9.504	-0.684	-9.881	0.051	0.051	Γ-Γ
CdTe	12.513	-9.517	-0.867	-10.033	0.052	0.052	Γ-Γ
GaAs	10.863	-54.896	-1.362	-55.859	0.009	0.009	Γ-Γ
GaN	8.598	-3.392	-0.555	-3.762	0.144	0.144	Γ-X
GaP	10.294	-4.565	-1.313	-5.514	0.230	1.062	Γ-Δ
SiC	8.277	-1.388	-0.844	-2.160	0.228	0.677	Γ-X
ZnS	10.286	-2.751	-0.694	-3.170	0.167	0.167	Γ-Γ
ZnSe	10.833	-5.340	-0.791	-5.834	0.089	0.089	Γ-Γ
ZnTe	11.682	-6.495	-1.032	-7.174	0.076	0.076	Γ-Γ
BaO	10.566	-0.216	-2.018	-2.018	0.380	1.197	X-X
CaO	9.121	-1.407	-0.174	-0.653	0.443	1.424	Γ-X
Li_2O	8.730	-0.540	-0.278	-0.747	0.437	0.850	Γ-X
MgO	8.037	-1.291	-0.231	-1.361	0.340	0.340	Γ-Γ
SrO	9.810	-1.519	-0.120	-0.625	0.407	1.225	Γ-X

TABLE S3: Calculated valence band ZPR for selected materials as in Miglio et al.[1] in the generalized Fröhlich formalism (ZPR_v^{gFr}) based on first principles GGA-PBE parameters. The materials considered contain triply degenerated valence bands coupled to one LO phonon branch, except BaO which consist of only one electronic band. The lattice types abbreviations correspond to zinc-blende(zb), respectively rocksalt(rs) thus falling in the cubic space group symmetry.

Material	Lattice	ω_{LO} (meV)	ε_∞	ε_0	ZPR_v^{gFr}(meV)
AlAs	zb	47.3	9.49	11.51	11.50
AlP	zb	59.9	8.12	10.32	20.56
AlSb	zb	39.8	12.02	13.35	4.00
BAs	zb	84.4	9.81	9.89	0.53
BN	zb	161.0	4.52	6.69	94.47
CdS	zb	34.4	6.21	10.24	38.73
CdSe	zb	23.6	7.83	11.78	19.69
CdTe	zb	19.1	8.89	12.37	11.91
GaAs	zb	33.5	15.31	17.55	3.27
GaN	zb	86.0	6.13	16.30	72.26
GaP	zb	48.6	10.50	11.00	8.46
SiC	zb	117.0	6.97	10.30	58.28
ZnS	zb	40.6	5.97	9.40	40.06
ZnSe	zb	29.3	7.35	10.73	21.69
ZnTe	zb	24.1	9.05	11.99	11.06
BaO	rs	47.3	4.21	92.43	225.34
CaO	rs	66.8	3.77	16.76	223.20
Li_2O	rs	86.3	2.9	7.8	364.59
MgO	rs	84.5	3.23	11.14	326.99
SrO	rs	55.4	3.77	20.91	228.95

TABLE S4: Convergence sampling used in the calculation of the self-energy term in the degenerate band scenario for 19 of the studied materials. $\partial^2\Sigma/\partial k^2$ was converged until a $1E-5$ Ha precision was reached.

Material	100			110			111		
	q	θ	ϕ	q	θ	ϕ	q	θ	ϕ
AlAs	240	240	240	144	144	144	128	128	128
AlP	144	144	144	144	144	144	144	144	144
AlSb	240	240	240	144	144	144	144	144	144
Bas	128	128	128	96	96	96	128	128	128
BN	240	240	240	128	128	128	128	128	128
CdS	320	320	320	240	240	240	240	240	240
CdSe	360	360	360	360	360	360	360	360	360
CdTe	360	360	360	360	360	360	360	360	360
GaAs	320	320	320	320	320	320	320	320	320
GaN	320	320	320	180	180	180	320	320	320
GaP	280	280	280	160	160	160	160	160	160
SiC	160	160	160	128	128	128	144	144	144
ZnS	280	280	280	180	180	180	280	280	280
ZnSe	240	240	240	160	160	160	240	240	240
ZnTe	280	280	280	160	160	160	160	160	160
CaO	360	360	360	360	360	360	360	360	360
Li2O	280	280	280	160	160	160	144	144	144
MgO	320	320	320	320	320	320	320	320	320
SrO	400	400	400	400	400	400	360	360	360

[1] A. Miglio, V. Brousseau-Couture, E. Godbout, G. Antonius, Y.-H. Chan, S. G. Louie, M. Côté, M. Giantomassi, and X. Gonze, npj Computational Materials **6**, 167 (2020).

TABLE S5: Second order derivative of the self-energy with respect to the wave-vector along different high-symmetry directions relevant to cubic materials. The quantity is calculated via a finite difference method around $k = 0$. The quantities are expressed in atomic units.

Material	$\partial^2\Sigma/\partial k^2$ (100)			$\partial^2\Sigma/\partial k^2$ (110)			$\partial^2\Sigma/\partial k^2$ (111)		
	1	**2**	**3**	**1**	**2**	**3**	**1**	**2**	**3**
AlAs	0.778	0.142	0.142	0.908	0.142	0.012	0.951	0.055	0.055
AlP	0.574	0.164	0.164	0.732	0.164	0.006	0.785	0.059	0.059
AlSb	0.442	0.078	0.078	0.512	0.078	0.008	0.536	0.031	0.031
BAs	0.008	0.006	0.006	0.014	0.006	0.000	0.016	0.002	0.002
BN	0.283	0.267	0.267	0.539	0.267	0.011	0.624	0.096	0.096
CdS	3.092	0.390	0.390	3.394	0.390	0.088	3.494	0.189	0.189
CdSe	6.059	0.416	0.416	6.330	0.416	0.145	6.421	0.236	0.236
CdTe	4.422	0.366	0.366	4.683	0.366	0.106	4.770	0.193	0.193
GaAs	4.596	0.149	0.149	4.671	0.149	0.073	4.696	0.099	0.098
GaN	2.086	0.286	0.286	2.324	0.286	0.048	2.404	0.127	0.127
GaP	0.510	0.120	0.120	0.620	0.120	0.010	0.657	0.046	0.046
SiC	0.431	0.224	0.224	0.656	0.224	-0.001	0.731	0.074	0.074
ZnS	1.732	0.353	0.353	2.038	0.353	0.047	2.140	0.149	0.149
ZnSe	2.762	0.345	0.345	3.040	0.345	0.068	3.132	0.160	0.160
ZnTe	2.072	0.276	0.276	2.300	0.276	0.048	2.377	0.124	0.124
CaO	2.551	0.176	0.176	2.019	0.708	0.176	1.842	0.531	0.531
Li2O	1.342	0.574	0.574	1.893	0.574	0.023	2.077	0.207	0.207
MgO	3.231	0.461	0.461	3.557	0.461	0.135	3.665	0.243	0.243
SrO	3.592	0.146	0.146	2.679	1.060	0.146	2.375	0.755	0.755

TABLE S6: Inverse of hole polaron effective masses associated with the triply degenerate valence bands along different crystallographic directions. The quantities are expressed in atomic units.

Material	$1/m^*_{pol}$ (100)			$1/m^*_{pol}$ (110)			$1/m^*_{pol}$ (111)		
AlAs	-8.583	-1.897	-1.897	-10.290	-1.897	-0.191	-10.859	-0.759	-0.759
AlP	-4.621	-1.623	-1.623	-6.095	-1.623	-0.150	-6.585	-0.641	-0.641
AlSb	-12.503	-2.667	-2.667	-14.853	-2.667	-0.317	-15.636	-1.100	-1.100
BAs	-4.666	-4.202	-4.202	-8.339	-4.202	-0.529	-9.563	-1.753	-1.753
BN	-1.551	-1.672	-1.672	-2.983	-1.672	-0.240	-3.461	-0.718	-0.718
CdS	-4.906	-0.821	-0.821	-5.531	-0.821	-0.195	-5.740	-0.404	-0.404
CdSe	-12.949	-0.951	-0.951	-13.738	-0.951	-0.161	-14.002	-0.424	-0.424
CdTe	-14.612	-1.367	-1.367	-15.735	-1.367	-0.245	-16.109	-0.619	-0.619
GaAs	-105.195	-2.576	-2.576	-107.445	-2.576	-0.326	-108.195	-1.076	-1.076
GaN	-4.699	-0.824	-0.824	-5.386	-0.824	-0.138	-5.615	-0.366	-0.366
GaP	-8.619	-2.506	-2.506	-10.771	-2.506	-0.354	-11.489	-1.071	-1.071
SiC	-2.346	-1.464	-1.464	-3.736	-1.464	-0.074	-4.199	-0.537	-0.537
ZnS	-3.770	-1.036	-1.036	-4.577	-1.036	-0.228	-4.847	-0.497	-0.497
ZnSe	-7.917	-1.237	-1.237	-8.925	-1.237	-0.229	-9.260	-0.565	-0.565
ZnTe	-10.918	-1.787	-1.787	-12.400	-1.787	-0.305	-12.894	-0.799	-0.799
BaO	-0.108	-0.108	0.589	-0.108	-0.108	0.589	-0.108	-0.108	0.589
CaO	-0.262	-0.171	-0.171	-0.215	-0.219	-0.171	-0.199	-0.203	-0.203
Li_2O	0.261	0.01903	0.019	0.327	0.019	-0.048	0.350	-0.025	-0.025
MgO	0.648	-0.002	-0.002	0.673	-0.002	-0.027	0.682	-0.018	-0.018
SrO	0.555	-0.094	-0.094	0.415	0.046	-0.094	0.369	-0.001	-0.001

TABLE S7: Ratio between the electronic effective mass and polaron effective mass along different directions in the studied cubic materials characteristic to the degenerate electronic bands case.

Material	$m_e/m^*_{pol}(100)$			$m_e/m^*_{pol}(110)$			$m_e/m^*_{pol}(111)$		
	1	**2**	**3**	**1**	**2**	**3**	**1**	**2**	**3**
AlAs	0.917	0.931	0.931	0.919	0.931	0.941	0.919	0.932	0.932
AlP	0.889	0.908	0.908	0.893	0.908	0.961	0.894	0.916	0.916
AlSb	0.966	0.972	0.972	0.967	0.972	0.976	0.967	0.972	0.972
BAs	0.998	0.999	0.999	0.998	0.999	1.000	0.998	0.999	0.999
BN	0.846	0.862	0.862	0.847	0.862	0.956	0.847	0.882	0.882
CdS	0.613	0.678	0.678	0.620	0.678	0.689	0.622	0.682	0.682
CdSe	0.681	0.696	0.696	0.685	0.696	0.526	0.686	0.643	0.643
CdTe	0.768	0.789	0.789	0.771	0.789	0.698	0.772	0.762	0.762
GaAs	0.958	0.945	0.945	0.958	0.945	0.816	0.958	0.916	0.916
GaN	0.693	0.742	0.742	0.699	0.742	0.743	0.700	0.742	0.742
GaP	0.944	0.954	0.954	0.946	0.954	0.973	0.946	0.958	0.958
SiC	0.845	0.867	0.867	0.851	0.867	1.017	0.852	0.879	0.879
ZnS	0.685	0.746	0.746	0.692	0.746	0.829	0.694	0.770	0.770
ZnSe	0.741	0.782	0.782	0.746	0.782	0.772	0.747	0.779	0.779
ZnTe	0.840	0.866	0.866	0.844	0.866	0.864	0.844	0.865	0.865
BaO	0.436	0.436	-0.254	0.436	0.436	-0.254	0.436	0.436	-0.254
CaO	0.093	0.493	0.493	0.096	0.236	0.493	0.097	0.277	0.277
Li2O	-0.241	-0.034	-0.034	-0.209	-0.034	0.675	-0.202	0.110	0.110
MgO	-0.251	0.003	0.003	-0.233	0.003	0.166	-0.228	0.070	0.070
SrO	-0.183	0.391	0.391	-0.183	-0.045	0.391	-0.184	0.001	0.001

TABLE 8.a: Hole polaron localization length determined in the studied materials along different high-symmetry directions relevant to cubic materials pertaining to the degenerate electronic bands case. The lengths are expressed as a function of the repetition distance between equivalent atoms in the unit cell. The repetition distance is mentioned in the last column.

Material	(100)			(110)			(111)			d(Bohr)
	a_1(d)	a_2(d)	a_3(d)	a_1(d)	a_2(d)	a_3(d)	a_1(d)	a_2(d)	a_3(d)	
AlAs	136.43	78.53	78.53	111.72	58.73	26.60	117.33	43.99	43.99	7.654
AlP	65.69	44.70	44.70	55.18	33.29	14.39	59.34	25.09	25.09	7.358
AlSb	383.71	218.69	218.69	318.70	166.61	80.08	331.38	124.90	124.90	8.317
BAs	3171.32	3054.42	3054.42	3197.80	2476.79	1203.92	3507.54	1894.29	1894.29	6.426
BN	20.64	21.05	21.05	21.63	17.32	8.50	23.85	13.28	13.28	4.770
CdS	28.93	14.56	14.56	25.23	11.97	7.27	25.30	9.23	9.23	7.921
CdSe	76.36	29.08	29.08	65.27	23.75	14.25	64.88	18.21	18.21	8.281
CdTe	104.33	43.43	43.43	88.54	35.02	20.29	88.49	26.67	26.67	8.848
GaAs	1797.95	455.74	455.74	1487.95	358.55	186.62	1486.37	267.94	267.94	7.681
GaN	28.82	14.93	14.93	24.40	11.79	6.38	24.80	8.91	8.91	6.080
GaP	185.63	118.34	118.34	159.89	92.27	46.69	166.52	69.59	69.59	7.279
SiC	31.24	26.13	26.13	26.66	18.54	6.27	30.82	14.39	14.39	5.853
ZnS	26.94	16.37	16.37	23.76	13.27	7.60	24.24	10.15	10.15	7.273
ZnSe	58.64	29.27	29.27	50.01	23.42	13.20	50.50	17.79	17.79	7.660
ZnTe	107.15	54.89	54.89	90.81	43.46	23.72	92.16	32.87	32.87	8.260
CaO	3.60	1.68	1.68	3.72	2.70	1.91	3.82	2.64	2.64	6.450
Li_2O	2.31	1.82	1.82	2.11	1.43	0.70	2.25	1.08	1.08	6.173
MgO	3.98	2.13	2.13	3.63	1.85	1.28	3.62	1.49	1.49	5.683
SrO	2.92	1.15	1.15	3.14	1.41	2.34	3.33	2.34	2.34	6.937

TABLE 8.b: Hole polaron formation energy in the strong coupling limit along different high-symmetry directions relevant to cubic materials pertaining to the degenerate electronic bands case.

	E_{SC}(meV)		
	(100)	(110)	(111)
AlAs	-0.13517	-0.20604	-0.19736
AlP	-0.37606	-0.57906	-0.54229
AlSb	-0.01994	-0.02958	-0.02875
BAs	-0.00023	-0.00031	-0.00029
BN	-3.90519	-5.22358	-4.90517
CdS	-2.27488	-3.01849	-3.07203
CdSe	-0.64406	-0.85738	-0.87593
CdTe	-0.31171	-0.42327	-0.43000
GaAs	-0.00694	-0.00960	-0.00966
GaN	-3.33710	-4.69221	-4.68922
GaP	-0.08218	-0.11823	-0.11551
SiC	-1.54667	-2.56839	-2.20181
ZnS	-2.30872	-3.13410	-3.14241
ZnSe	-0.78833	-1.08677	-1.09486
ZnTe	-0.24936	-0.34915	-0.34961
CaO	-75.87667	-62.73596	-57.15204
Li2O	-96.31797	-137.12446	-131.20188
MgO	-77.31154	-95.18113	-97.82699
SrO	-101.31612	-75.53183	-64.65848

TABLE S9: Electron polaron localization length expressed in units of the repetition distance between equivalent atoms. a_p(d) is the spherical average determined by Eq. 108 where the electronic effective masses expressed in Table S2 have been used. $a_{p\perp}$ is the in-plane localization length. a_{pz} is the out-of-plane localization length. The radii are determined in the Fröhlich model.

Material	a_p(d)	$a_{p\perp}$(d)	a_{pz}(d)	Ratio	Shape
AlAs	13.81	16.10	10.15	0.63	oblate
AlN	28.70	30.39	25.59	0.84	oblate
AlP	12.04	13.81	9.14	0.66	oblate
AlSb	18.92	22.94	12.87	0.56	oblate
BAs	259.24	313.63	177.12	0.56	oblate
BN	6.37	7.25	4.92	0.68	oblate
CdS	63.62	-	-	-	spherical
CdSe	207.27	-	-	-	spherical
CdTe	259.36	-	-	-	spherical
GaAs	6439.74	-	-	-	spherical
GaN	59.65	59.65	59.65	1.00	spherical
GaP	13.15	15.75	9.17	0.58	oblate
SiC	10.67	12.14	8.26	0.68	oblate
ZnS	50.60	-	-	-	spherical
ZnSe	128.23	-	-	-	spherical
ZnTe	219.80	-	-	-	spherical
BaO	1.09	1.24	0.83	0.67	oblate
CaO	1.04	1.19	0.79	0.66	oblate
Li2O	2.37	2.57	2.03	0.79	oblate
MgO	7.26	-	-	-	spherical
SrO	0.98	1.11	0.75	0.68	oblate

TABLE S10: Electron polaron localization length expressed in units of the repetition distance between equivalent atoms. a_p(d) is the spherical average determined by Eq. 37 where the electronic effective masses expressed in Table S2 have been used. $a_{p\perp}$ is the in-plane localization length. a_{pz} is the out-of-plane localization length. The radii are determined in the Feynman model.

Material	a_p(d)	$a_{p\perp}$(d)	a_{pz}(d)	Ratio	Shape
AlAs	16.72	28.72	5.66	0.20	oblate
AlP	13.96	22.64	5.31	0.23	oblate
AlSb	23.26	45.97	5.96	0.13	oblate
BAs	81.55	160.16	21.14	0.13	oblate
BN	8.57	13.47	3.47	0.26	oblate
CdS	40.82	-	-	-	spherical
CdSe	146.15	-	-	-	spherical
CdTe	164.80	-	-	-	spherical
GaAs	2783.85	-		-	spherical
GaN	30.76	-	-	-	spherical
GaP	18.62	35.14	5.23	0.15	oblate
SiC	13.11	20.55	5.33	0.26	oblate
ZnS	28.07	-	-	-	spherical
ZnSe	74.74	-	-	-	spherical
ZnTe	110.51	-	-	-	spherical
BaO	3.36	5.34	1.32	0.25	oblate
CaO	3.03	4.86	1.18	0.24	oblate
Li2O	3.58	4.68	2.09	0.45	oblate
MgO	6.91	-	-	-	spherical
SrO	3.30	5.15	1.35	0.26	oblate

TABLE S11: Calculated conduction band ZPR for selected materials as in Miglio et al.[1] in the generalized Fröhlich formalism (ZPR_v^{gFr}) based on first principles GGA-PBE parameters and compared to the Feynman variational approach for both isotropic and anisotropic non-degenerate electronic bands.

Material	Fröhlich	Feynman			R.E.(%)
	ZPR_c^{gFr}(meV)	F_{avg}(meV)	$F_\perp$(meV)	F_z(meV)	
AlAs	-8.8	-9.6	-7.3	-14.1	-9.4%
AlP	-14.0	-15.1	-11.9	-21.4	-7.6%
AlSb	-3.6	-4.1	-2.9	-6.5	-15.0%
BAs	-0.5	-0.6	-0.4	-0.9	-14.2%
BN	-67.9	-72.6	-58.3	-101.3	-7.0%
CdS	-14.9	-15.0	-15.0	-15.0	-0.5%
CdSe	-5.5	-5.5	-5.5	-5.5	-0.3%
CdTe	-3.7	-3.7	-3.7	-3.7	-0.3%
GaAs	-0.5	-0.5	-0.5	-0.5	0.4%
GaN	-29.6	-29.7	-29.7	-29.7	-0.4%
GaP	-7.4	-8.3	-6.0	-13.0	-13.0%
SiC	-32.7	-34.8	-28.0	-48.4	-6.6%
ZnS	-18.6	-18.7	-18.7	-18.7	-0.6%
ZnSe	-8.1	-8.1	-8.1	-8.1	-0.3%
ZnTe	-4.3	-4.3	-4.3	-4.3	-0.2%
BaO	-132.0	-148.2	-115.9	-212.7	-12.3%
CaO	-153.9	-171.2	-133.7	-246.1	-11.3%
Li2O	-171.7	-180.8	-159.1	-224.2	-5.3%
MgO	-137.3	-140.4	-140.4	-140.4	-2.2%
SrO	-141.0	-156.5	-124.1	-221.3	-11.0%

TABLE S12: Calculated conduction band polaron effective masses for selected materials as in Miglio et al.[1] in the generalized cubic Fröhlich formalism based on first principles GGA-PBE parameters and compared to the Feynman variational approach for both isotropic and anisotropic non-degenerate electronic bands.

Material	Fröhlich		Feynman		R.E.	
	$m^*_{pol_\perp}$[a.u.]	$m^*_{pol_z}$[a.u.]	$m^*_{pol_\perp}$[a.u.]	$m^*_{pol_z}$[a.u.]	/$m^*_{pol_\perp}$[a.u.]	$m^*_{pol_z}$[a.u.]
AlAs	0.25181	0.91550	0.24901	0.94087	1.1%	-2.8%
AlP	0.26372	0.83222	0.26024	0.85736	1.3%	-3.0%
AlSb	0.22561	1.15212	0.22422	1.17299	0.6%	-1.8%
BAs	0.21668	1.09474	0.21660	1.09608	0.0%	-0.1%
BN	0.32467	0.94301	0.31661	0.98838	2.5%	-4.8%
CdS	0.12688	0.12688	0.12622	0.12622	0.5%	0.5%
CdSe	0.05322	0.05322	0.05313	0.05313	0.2%	0.2%
CdTe	0.05349	0.05349	0.05344	0.05344	0.1%	0.1%
GaAs	0.00914	0.00914	0.00914	0.00914	0.0%	0.0%
GaN	0.15229	0.15228	0.15179	0.15179	0.3%	0.3%
GaP	0.23670	1.07856	0.23431	1.10864	1.0%	-2.8%
SiC	0.24090	0.70067	0.23723	0.72354	1.5%	-3.3%
ZnS	0.18094	0.18094	0.17989	0.17989	0.6%	0.6%
ZnSe	0.09362	0.09362	0.09343	0.09343	0.2%	0.2%
ZnTe	0.07877	0.07877	0.07871	0.07871	0.1%	0.1%
BaO	0.81412	1.78651	0.53076	2.03669	34.8%	-14.0%
CaO	0.79178	1.95175	0.58676	2.25404	25.9%	-15.5%
Li2O	0.68378	1.17113	0.56847	1.20511	16.9%	-2.9%
MgO	0.46571	0.46571	0.43153	0.43153	7.3%	7.3%
SrO	0.78801	1.76349	0.55448	1.99554	29.6%	-13.2%

TABLE S13: Feynman path integral variational method parameters for the non-degenerate anisotropic case.

Materials	$v_\perp$	$w_\perp$	v_z	w_z
AlAs	3.01564	2.98092	3.03038	2.96301
AlP	3.02014	2.97542	3.03662	2.95554
AlSb	3.00726	2.99193	3.01659	2.97979
BAs	3.00054	2.99946	3.00569	3.00326
BN	3.03711	2.95497	3.06588	2.92091
CdS	3.04481	2.94577	3.04481	2.94576
CdSe	3.02365	2.97114	3.02366	2.97114
CdTe	3.01950	2.97622	3.01949	2.97621
GaAs	3.00178	2.99821	3.00474	3.00117
GaN	3.03537	2.95703	3.03537	2.95703
GaP	3.01381	2.98608	3.02714	2.96694
SiC	3.02434	2.97036	3.04256	2.94843
ZnS	3.04752	2.94256	3.04751	2.94255
ZnSe	3.02819	2.96567	3.02819	2.96567
ZnTe	3.01804	2.97800	3.01805	2.97801
BaO	3.30498	2.66690	3.72792	2.32391
CaO	3.23770	2.73342	3.53099	2.46877
Li2O	3.21540	2.75629	3.32837	2.64464
MgO	3.19076	2.78207	3.19075	2.78206
SrO	3.27253	2.69853	3.60088	2.41464

TABLE S14: Cs_2NaScF_6 hole and electron polaron characteristics, respectively effective masses and localization lengths, along 3 crystallographic directions.

Luttinger Parameters	0.02891	0.07544	0.00377
CB electron effective mass			
(100)	17.293	6.628	6.628
(110)	9.942	9.942	6.628
(111)	8.521	8.521	8.007
Electron polaron effective mass			
(100)	-11.992	-2.518	-2.518
(110)	-3.399	-3.949	-2.518
(111)	-3.522	-3.522	-3.227
Localization length (d)			
(100)	0.16	0.23	0.23
(110)	0.20	0.20	0.23
(111)	0.22	0.22	0.22
E_{SC}(meV)			
(100)	-1365.54		
(110)	-1299.45		
(111)	-1284.82		

Luttinger parameters	-0.00205	-0.08035	-0.01328
VB electron effective mass			
(100)	-243.704	-6.223	-6.223
(110)	-14.467	-10.451	-6.223
(111)	-10.035	-10.035	-7.923
Hole polaron effective mass			
(100)	1.417	1.417	265.341
(110)	1.417	2.382	3.452
(111)	1.791	2.335	2.335
Localization length (d)			
(100)	0.05	0.17	0.17
(110)	0.16	0.18	0.22
(111)	0.19	0.19	0.21
E_{SC}(meV)			
(100)	-2222.08		
(110)	-1483.25		
(111)	-1425.88		

Dielectric coupling		
Mode	Frequency	ϵ^*
12	13.05	36.64
18	22.94	11.03
24	31.98	20.43
30	57.77	6.26